Stokes scintillations for vector vortex beams with controllable spatial correlation

Manisha,[1,*,†] Hemant Kumar Singh,[1,*] P. Senthilkumaran,[1,2] and Bhaskar Kanseri[1,2]
[1]*Department of Physics, Indian Institute of Technology Delhi, Hauz Khas, New Delhi 110016, India*
[2]*Optics and Photonics Centre, Indian Institute of Technology Delhi, Hauz Khas, New Delhi 110016, India*

(Received 21 December 2023; accepted 27 March 2024; published 16 April 2024)

The present work reports the theoretical and experimental observation of Stokes scintillations (SS) for focused vector vortex beams (VVBs) with controllable spatial correlation. Initially, a Gaussian-Schell model (GSM) source is utilized to generate the partially coherent VVBs (PC-VVBs). The focusing of PC-VVBs results in the optimization of extremum values of SS parameters across the beam cross section. Additionally, the SS parameters of the focused PC-VVB show spatially structured behavior. It is found that the spatial correlation, the inhomogeneous polarization distribution, and the Poincaré-Hopf index (PHI) of VVBs are important factors for structuring the SS parameters. The SS parameters are observed to exhibit a complementary relationship. Furthermore, the degeneracy associated with the SS parameters is discussed to complete the study. The flower-patterned distribution of specific SS parameters is useful in determining the topological index of the PC-VVBs. Interestingly, the bound condition and complementary nature of SS parameters are useful for scintillation squeezing across the beam cross section in PC-VVBs, where one SS parameter is suppressed at the expense of another. Thus, the source can be finely tuned using the bound condition with correlation and topological features to harness this effect optimally.

DOI: 10.1103/PhysRevA.109.043516

I. INTRODUCTION

Polarization in the electromagnetic (EM) field denotes the correlation observed between the orthogonal electric field components at a specific space-time coordinate. Similarly, spatial correlation characterizes the degree of correlation between electric field components at two distinct transverse points within the EM field [1]. Whenever an EM beam propagates through any random media, its coherence, polarization, and intensity (beam profile) fluctuate due to the randomness of the medium. The fluctuations in intensity are of particular interest because their correlations help to determine the unknown source properties. Hanbury Brown and Twiss (HBT) first studied these fluctuation correlations in the scalar fields to determine the angular diameter of distant celestial objects [2–4]. Since then, the HBT effect has been applied to nuclear physics [5], classical optics [6,7], quantum optics [8], and so on. However, due to their wide applications in multiple domains of physics, the effect was mainly restricted to the scalar optical fields. Recently, it has been observed that the subtle correlations of the fields must be addressed for the electromagnetic optical field [9]. This leads to Stokes fluctuation correlations or generalization of the HBT effect. These correlations in Stokes parameters at a single spatial point are known as Stokes scintillations (SS) and are useful in explaining light-matter interaction [10], semiconductor lasers [11], beam propagation [12], etc. Scintillations are essential to investigate because they are a source of signal degradation quantifiable by the elements of the 4×4 SS matrix. Under the assumption of Gaussian statistics, the diagonal SS parameters are found to be bounded by a sum rule. They can be manipulated across the beam cross section by controlling the coherence and polarization properties of the source. It implies that an increase (decrease) in a particular SS parameter is accompanied by a decrease (increase) in the other SS parameters at the same point. Depending on the type of application, it may be preferable to tune the SS parameters. For example, the first SS parameter results from a speckle pattern. So, optimizing the level of the first SS parameter can be helpful in free space and laser communications through the turbulent atmosphere [13]. Similarly, other SS parameters are polarization dependent, which enables tunability of different polarizations depending upon their applications. One of the effective ways to control the scintillations is using a spatially partially coherent (PC) beam. It was found that the intensity and polarization-resolved scintillations and phase distortion caused by fluctuating light fields are reduced for PC fields, which leads to a decrease in communication error rate and an increase in the channel capacity [13,14]. The interconnection between coherence and polarization is anticipated to cause modulation in either property by altering the correlation within fluctuating fields in standard Gaussian beams, Laguerre-Gaussian beams, Bessel beams, partially coherent vector vortex beams (PC-VVBs), etc. [15–19]. Hence, PC-VVBs are an appropriate field structure for investigating polarization-resolved intensity fluctuations.

The VVBs are polarization-structured beams with an undefined azimuth and intensity null at the vortex center [20]. The characterizing parameter of such a beam is PHI ($\eta = \frac{1}{2\pi}\oint \nabla\Phi \cdot dl$), where $\nabla\Phi$ gives the gradient of polarization

*These authors contributed equally to this work.
†manisha12101994@gmail.com

azimuth in the immediate neighborhood of the vortex center. Interestingly, the VVBs of a particular η have polarization distributions identical to the fiber modes and can also be generated readily using laser resonators [21]. Most of the practical applications of these beams in a fully coherent regime are associated with their orbital angular momentum (OAM) and spin angular momentum (SAM) states [20,22,23]. However, simultaneous research progress asserts that VVBs in partially coherent regimes enhance the capability of particular applications such as robustness in communication ($\sim$ two times) [24,25], speckle-free and enhanced image contrast [13,26], trapping of particles with different refractive indices [22], and so on. Furthermore, it was found that the PHI of VVBs is a stable quantity and provides a reduced level of intensity degradation on propagation [27,28]. Additionally, PC-VVBs with controlled correlations and topological characteristics offer the capability for beam shaping, self-focusing, and self-rotation [19,29–31], which renders them valuable for sculpting the illuminating beam to reduce fluctuations [32,33]. This has indeed led to a growing emphasis on PC-VVBs in the direction of optimizing polarization-resolved intensity fluctuations. Most of the research related to scintillation is confined to random EM beams [9,34,35], although there is a recent report on the stability of polarization-dependent Stokes parameters over the intensity distribution for radially polarized VVB [36]. However, the SS parameters for both generic and higher-order PC-VVBs and their dependency on the topology have not yet been explored.

In this article, we present theoretically and experimentally the effect of input spatial correlation and PHI on controlling the Stokes scintillations for focused PC-VVBs. The Gaussian-Schell model (GSM) beam is considered for both experiment and theory purposes. The diagonal elements of the SS matrix, which give the variance of Stokes parameters, are explored in this work. Although it was found that focusing produces a significant increase in the scintillation index of electromagnetic beams [37], the present work shows that the maximum value of the first SS parameter (scintillation index) for PC-VVBs at the source plane can be manipulated upon focusing. Further, the spatial distribution of other SS parameters for focused PC-VVBs demonstrates an unexpected spatial behavior. Moreover, we found that the focusing of PC-VVB results in a substantial increment and decrement of the maximum value of SS parameters when compared with their counterparts at the source plane. These manifold characteristics of focused PC-VVBs and the sum rule of SS parameters open up the possibility of an analogous term used in the quantum domain, i.e., "scintillation squeezing." This involves the suppression of specific Stokes scintillations at the expense of others. Thus, depending upon the choice of application, one can tune the scintillations accordingly. In Secs. II and III, the mathematical preliminaries are explained to deduce the SS parameters of focused PC-VVBs. The theoretical formalism predicts that the spatial distribution and strength of SS parameters are fundamentally dependent on the PHI and spatial correlation width of the input beam. The experimental setup to synthesize the focused PC-VVBs to study their scintillation properties is given in Sec. IV. The experimental results with their theoretical predictions are discussed in Sec. V. Section VI concludes all the key findings of the paper.

II. THE STOKES SCINTILLATIONS

Based upon the unified theory [1], the correlation and polarization properties of a random, statistically stationary (in a wide sense) partially coherent electromagnetic beam can be characterized using 2×2 cross-spectral density (CSD) matrix as

$$\mathbf{W}(\mathbf{r}_1, \mathbf{r}_2) = \begin{pmatrix} W_{xx}(\mathbf{r}_1, \mathbf{r}_2) & W_{xy}(\mathbf{r}_1, \mathbf{r}_2) \\ W_{yx}(\mathbf{r}_1, \mathbf{r}_2) & W_{yy}(\mathbf{r}_1, \mathbf{r}_2) \end{pmatrix}, \tag{1}$$

where $W_{\alpha\beta}(\mathbf{r}_1, \mathbf{r}_2) = \langle E^*_\alpha(\mathbf{r}_1) E_\beta(\mathbf{r}_2)\rangle$, $(\alpha, \beta = x, y)$ is the first-order correlation between electric fields at two spatial points $\mathbf{r}_1(r_1, \theta_1)$ and $\mathbf{r}_2(r_2, \theta_2)$. Any state of polarization of an EM beam can be defined in terms of the single-point Stokes parameter. The instantaneous value of Stokes parameters at a spatial point $\mathbf{r}$ can be given in terms of electric field components $E_x(\mathbf{r})$ and $E_y(\mathbf{r})$ as

$$\begin{aligned} S_0(\mathbf{r}) &= E^*_x(\mathbf{r})E_x(\mathbf{r}) + E^*_y(\mathbf{r})E_y(\mathbf{r}), \\ S_1(\mathbf{r}) &= E^*_x(\mathbf{r})E_x(\mathbf{r}) - E^*_y(\mathbf{r})E_y(\mathbf{r}), \\ S_2(\mathbf{r}) &= E^*_x(\mathbf{r})E_y(\mathbf{r}) + E^*_y(\mathbf{r})E_x(\mathbf{r}), \\ S_3(\mathbf{r}) &= i[E^*_y(\mathbf{r})E_x(\mathbf{r}) - E^*_x(\mathbf{r})E_y(\mathbf{r})]. \end{aligned} \tag{2}$$

Taking the average on both sides, Eq. (2) reduces to Stokes parameters in relation to CSD elements as [38]

$$\begin{aligned} \langle S_0(\mathbf{r})\rangle &= W_{xx}(\mathbf{r}, \mathbf{r}) + W_{yy}(\mathbf{r}, \mathbf{r}), \\ \langle S_1(\mathbf{r})\rangle &= W_{xx}(\mathbf{r}, \mathbf{r}) - W_{yy}(\mathbf{r}, \mathbf{r}), \\ \langle S_2(\mathbf{r})\rangle &= W_{xy}(\mathbf{r}, \mathbf{r}) - W_{yx}(\mathbf{r}, \mathbf{r}), \\ \langle S_3(\mathbf{r})\rangle &= i[W_{yx}(\mathbf{r}, \mathbf{r}) - W_{xy}(\mathbf{r}, \mathbf{r})]. \end{aligned} \tag{3}$$

Similar to the intensity correlation in the scalar beams, the polarization-resolved intensity correlations were introduced using Stokes parameters [9]. For any stochastic EM field, the above parameters are random quantities; hence, fluctuations in these parameters are defined as

$$\Delta S_n(\mathbf{r}) = S_n(\mathbf{r}) - \langle S_n(\mathbf{r})\rangle, n = 0, 1, 2, 3. \tag{4}$$

Further, the correlations in the fluctuations of Stokes parameters are compiled in a 4×4 Stokes fluctuation (SF) matrix with elements [9]

$$\begin{aligned} C_{nm}(\mathbf{r}_1, \mathbf{r}_2) &= \langle \Delta S_n(\mathbf{r}_1)\Delta S_m(\mathbf{r}_2)\rangle, (n, m = 0 - 3) \\ &= \langle S_n(\mathbf{r}_1)S_m(\mathbf{r}_2)\rangle - \langle S_n(\mathbf{r}_1)\rangle\langle S_m(\mathbf{r}_2)\rangle. \end{aligned} \tag{5}$$

Under the assumption that the source follows Gaussian statistics, the SS parameters can be expressed in terms of CSD elements as [39]

$$\begin{aligned} C_{nm}(\mathbf{r}_1, \mathbf{r}_2) = \Sigma_{ab}\, \Sigma_{cd}\, \sigma^n_{ab}\, \sigma^m_{cd}\, W_{ad}(\mathbf{r}_1, \mathbf{r}_2) W^*_{bc}(\mathbf{r}_1, \mathbf{r}_2), \\ \text{with } (a, b, c, d = x, y). \end{aligned} \tag{6}$$

When the two spatial coordinates coincide, i.e., $(\mathbf{r}_1 = \mathbf{r}_2 = \mathbf{r})$, the SF matrix converts into the SS matrix with elements

$$\mathrm{D}_{nm}(\mathbf{r}) = C_{nm}(\mathbf{r}, \mathbf{r}). \tag{7}$$

The diagonal elements for the SS matrix measure the variance of Stokes parameters in fluctuating fields, and their decrement indicates the stability of Stokes parameters. Using Eqs. (5) and (6), the general expressions for normalized diagonal SS parameters are given as

$$\mathrm{D}_{00}^{N} = \frac{|W_{xx}|^2 + |W_{xy}|^2 + |W_{yx}|^2 + |W_{yy}|^2}{|W_{xx} + W_{yy}|^2}, \tag{8a}$$

$$\mathrm{D}_{11}^{N} = \frac{|W_{xx}|^2 - |W_{xy}|^2 - |W_{yx}|^2 + |W_{yy}|^2}{|W_{xx} + W_{yy}|^2}, \tag{8b}$$

$$\mathrm{D}_{22}^{N} = \frac{2\mathrm{Re}[W_{xx}W_{yy}^{*} + W_{xy}W_{yx}^{*}]}{|W_{xx} + W_{yy}|^2}, \tag{8c}$$

$$\mathrm{D}_{33}^{N} = \frac{2\mathrm{Re}[W_{xx}W_{yy}^{*} - W_{xy}W_{yx}^{*}]}{|W_{xx} + W_{yy}|^2}. \tag{8d}$$

III. PARTIALLY COHERENT VECTOR VORTEX BEAM

The electric field for a VVB can be written as a superposition of OAM states in orthogonal SAM states as [20]

$$E(\rho, \phi) = \frac{\rho^{|q|}}{2}\exp\left(-\frac{\rho^2}{4w^2}\right)[e^{iq\phi}\hat{L} + e^{-i(q\phi+\phi_0)}\hat{R}], \tag{9}$$

where $\rho^2 = \rho_x^2 + \rho_y^2; \phi = \arctan(\rho_y/\rho_x)$ is the azimuthal angle; w is the beam waist; q is the topological charge; and $\hat{L}$ and $\hat{R}$ are orthogonal basis vectors. Here, q determines the strength of the phase gradient of the OAM states and can take any integral value. For a PHI, η (such that $|\eta| = |q|$), there are two pairs of orthogonal basis states for VVBs: type I and type III with $+\eta$; and type II and type IV with $-\eta$ [20,40]. The first pair of inhomogeneously polarized orthogonal fields can be obtained by substituting $\phi_0 = 0$ and $\phi_0 = \pi$, while the other pair with negative $|\eta|'$s can be obtained by interchanging the OAM states of orthogonal polarization components. The PC-VVB is generated using the GSM-type source having beam waist w and spatial correlation width δ [39]. For PC-VVB of type I, the CSD matrix elements at the source plane ($W_{0\alpha\beta}$) are [31]

$$W_{0xx}(\boldsymbol{\rho}_1, \boldsymbol{\rho}_2) = \frac{(\rho_1\rho_2)^{|q|}}{(2w)^{2|q|}}\cos(q\phi_1)\cos(q\phi_2)\,\gamma(\boldsymbol{\rho}_1, \boldsymbol{\rho}_2), \tag{10a}$$

$$W_{0xy}(\boldsymbol{\rho}_1, \boldsymbol{\rho}_2) = \frac{(\rho_1\rho_2)^{|q|}}{(2w)^{2|q|}}\cos(q\phi_1)\sin(q\phi_2)\,\gamma(\boldsymbol{\rho}_1, \boldsymbol{\rho}_2), \tag{10b}$$

$$W_{0yx}(\boldsymbol{\rho}_1, \boldsymbol{\rho}_2) = \frac{(\rho_1\rho_2)^{|q|}}{(2w)^{2|q|}}\sin(q\phi_1)\cos(q\phi_2)\,\gamma(\boldsymbol{\rho}_1, \boldsymbol{\rho}_2), \tag{10c}$$

$$W_{0yy}(\boldsymbol{\rho}_1, \boldsymbol{\rho}_2) = \frac{(\rho_1\rho_2)^{|q|}}{(2w)^{2|q|}}\sin(q\phi_1)\sin(q\phi_2)\,\gamma(\boldsymbol{\rho}_1, \boldsymbol{\rho}_2), \tag{10d}$$

where $\gamma(\boldsymbol{\rho}_1, \boldsymbol{\rho}_2) = \exp[-\frac{\rho_1^2+\rho_2^2}{4w^2}]\exp[-\frac{(\rho_1-\rho_2)^2}{2\delta^2}]$, and $\boldsymbol{\rho}_1(\rho_1, \phi_1)$ and $\boldsymbol{\rho}_2(\rho_2, \phi_2)$ describe the position of two transverse points in the source plane. Using Eqs. (10a)–(10d) in the expressions mentioned in Eqs. (8a)–(8d), one can find the normalized SS parameters in the source plane as

$$\begin{aligned} \mathrm{D}_{00}^{N(s)} &= 1, \\ \mathrm{D}_{11}^{N(s)} &= \cos^2(2q\phi), \\ \mathrm{D}_{22}^{N(s)} &= \sin^2(2q\phi), \\ \mathrm{D}_{33}^{N(s)} &= 0. \end{aligned} \tag{11}$$

The above expressions show that the SS parameters for PC-VVB are independent of the radial coordinate, but some of the SS parameters depend on the azimuthal angle and topological charge. This is due to the azimuthal phase gradient on the spatially varying half-wave plate (SWP), which is used to generate the VVB given in Eq. (9). The SWP embeds requisite polarization distribution on the input beam, which will be discussed further in Sec. IV. It can be obtained easily that these parameters obey the sum rule, i.e.,

$$\sum_{n=0}^{3} \mathrm{D}_{nn}^{N(s)} = 2. \tag{12}$$

Figure 1 infers the variation of the normalized SS parameter for various index PC-VVBs at the source plane. The complementary nature of $\mathrm{D}_{00}^{N(s)}/\mathrm{D}_{11}^{N(s)}$ and $\mathrm{D}_{33}^{N(s)}/\mathrm{D}_{22}^{N(s)}$ is clear from Eq. (11). It is observed that at the source plane, $\mathrm{D}_{00}^{N(s)}$ and $\mathrm{D}_{33}^{N(s)}$ are independent of azimuthal angle and represent the concentric circles of radius 1 and 0, respectively, but $\mathrm{D}_{11}^{N(s)}$ and $\mathrm{D}_{22}^{N(s)}$ depend on the azimuthal angle. This means that the intensity scintillations are constant and maximum while polarization-resolved scintillations vary at the source plane for PC-VVBs. $\mathrm{D}_{11}^{N(s)}$ and $\mathrm{D}_{22}^{N(s)}$ possess a petal-like structure and the number of petals (K) gives the information about the topological index (q) of the SWP such that ($|q| = K/4$). Notably, the degree of polarization of the generated beam at the source plane is unity all across the beam cross section. It was obtained that a partially coherent, fully polarized beam always produces a maximum scintillation, i.e., "1" [37]. Hence, the modulation in the SS values at the source plane is the consequence of the topological index of the generated PC-VVB.

In this study, we aim to find the effect of focusing on the SS parameters for PC-VVBs of various indices. The effect of focusing on the statistical properties such as beam profile [41], spectral degree of coherence [42], and degree of polarization [43] of stochastic wave field are well known. Furthermore, the spatial behavior of stochastic structured light fields such as PC-VVBs exhibits even more intricate characteristics upon focusing. Hence, the generated PC-VVB is focused using a converging lens with the source and observation planes at the front and back focal planes, respectively, i.e., the field at the observation plane is proportional to the Fourier transform of the field at the source plane [44]. A similar relation holds for the CSD matrix elements focused with a lens (f) [16]

$$\begin{aligned} W_{\alpha\beta}(\mathbf{r}_1, \mathbf{r}_2, f) = \frac{k^2}{4\pi^2 f^2}\int_0^{\infty}\int_0^{\infty}\int_0^{2\pi}\int_0^{2\pi} W_{0\alpha\beta}(\boldsymbol{\rho}_1, \boldsymbol{\rho}_2) \\ \times \exp\left[\frac{ik}{f}(\boldsymbol{\rho}_1 \cdot \mathbf{r}_1 - \boldsymbol{\rho}_2 \cdot \mathbf{r}_2)\right]\rho_1\rho_2 d\rho_1\, d\rho_2 \\ \times\, d\phi_1\, d\phi_2, \end{aligned} \tag{13}$$

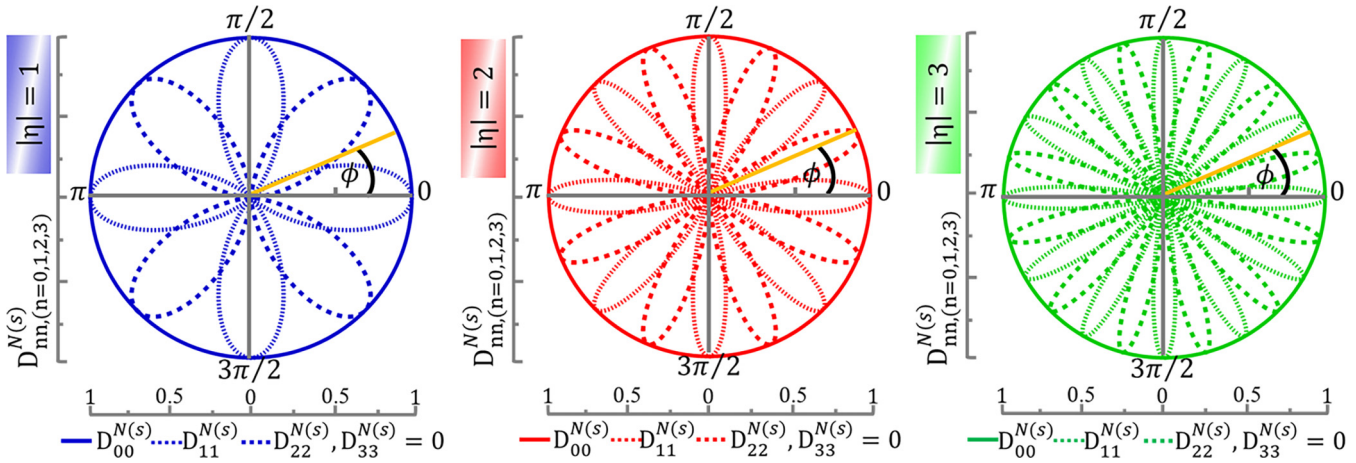

FIG. 1. The azimuthal variation of SS parameters $D^{N(s)}_{nn}$, $n = 0$ (solid line), 1 (dotted line), and 2 (dashed line) for PC-VVBs with $|\eta| = 1$ (blue), $|\eta| = 2$ (red), and $|\eta| = 3$ (green) at the source plane (SWP plane). Here, $D^{N(s)}_{00} = 1$ and $D^{N(s)}_{33} = 0$ (concentric circles of radius = 1 and = 0, respectively, for all indices).

where $k = \frac{2\pi}{\lambda}$, λ is free-space wavelength. The CSD matrix elements for type I PC-VVB at the back focal plane of the paraxial lens obtained upon solving Eq. (13) are given in Appendix. Using Eqs. (A1)–(A4) from Appendix A in Eqs. (8a)–(8d), one can obtain the diagonal SS parameters for PC-VVBs of various indices across the focal plane.

In Fig. 2, we have plotted SS parameters of a focused PC-VVB ($|\eta| = 1, 2, 3$) as a function of spatial correlation width (δ). The insets show their density profiles for two different δ values. Although the variation of D^N_{00} and D^N_{33} is identical to D^N_{11} and D^N_{22}, respectively, the two figures are shown to look into all four parameters separately. The azimuthally symmetric and asymmetric distribution of SS parameters is due to the inhomogeneous polarization distribution. It is observed that the variation of SS parameters D^N_{00} and D^N_{33} is complementary to each other, which is clear from their respective color maps also. However, the color map of the other two SS parameters D^N_{11} and D^N_{22} are identical, but their variation is complementary. For instance, the SS parameters corresponding to δ_1 and δ_2 are mentioned in Table I. It is seen that $D^N_{00}(f)$ can be lowered significantly by decreasing δ and increasing $|\eta|$. However, this leads to an increase of $D^N_{33}(f)$. A similar conflict is employed for the other two SS parameters. The SS parameters are equal for less correlated fields, and this deterioration is more for higher-index PC-VVBs. Reduction in δ at the source plane results in a decrease in the polarized contribution [degree of polarization (DOP, **P**)] across the focal plane [19,31]. Also, it was found that for uncorrelated fields ($\mathbf{P} = 0$), the SS parameters are equal [34]. However, for large δ, the identical SS parameters are nearly independent of the topological index of the input beam. By tuning the various source parameters, one can design a focused vector field in which the polarization-resolved intensity fluctuations are minimized, which can be useful in various applications such as communication, optical measurement, etc.

IV. THE EXPERIMENT

The experimental setup to generate the PC-VVB is presented in Fig. 3. A linearly polarized He-Ne laser beam is collimated with the help of microscope objective (MO), pinhole (PH), and lens L_1. The collimated beam is made to fall on

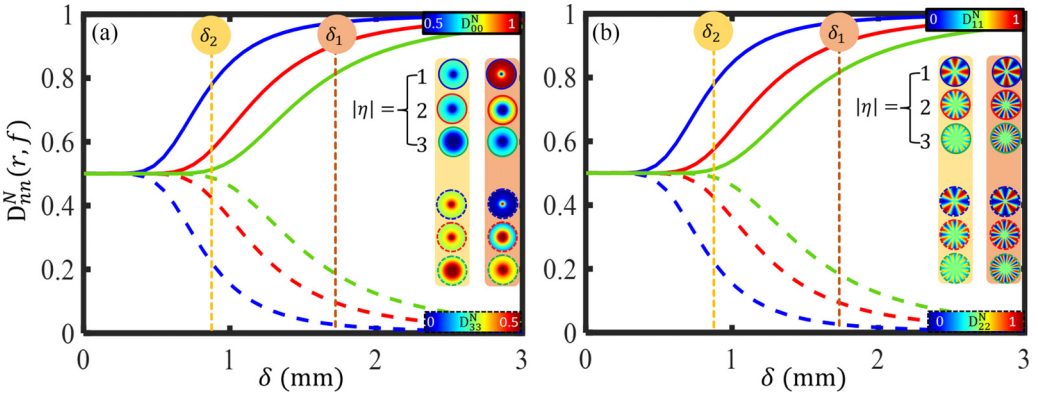

FIG. 2. Theoretical plot for the dependency of the SS parameters on correlation width δ of focused ($f = 200$ mm) PC-VVBs [$|\eta| = 1$ (blue), 2 (red), 3 (green)] at (0.5 mm, 0 mm). The selected location aligns with the extremum value (either maximum or minimum) of the SS parameters at the periphery of PC-VVB with a beam waist of 3 mm. (A) The solid lines represent D^N_{00} and dashed lines represent D^N_{33}. (B) The solid lines represent D^N_{11} and dashed lines represent D^N_{22}. In the insets the SS profiles corresponding to two distinct δ's (δ_1, δ_2) are shown.

TABLE I. The SS parameters for various index PC-VVBs with $|\eta| = 1, 2, 3$ at $\delta_1 = 1.54$ mm and $\delta_2 = 0.85$ mm.

	$\delta_1 = 1.54$ mm				$\delta_2 = 0.85$ mm			
$\lvert\eta\rvert$	$D^N_{00}(f)$	$D^N_{11}(f)$	$D^N_{22}(f)$	$D^N_{33}(f)$	$D^N_{00}(f)$	$D^N_{11}(f)$	$D^N_{22}(f)$	$D^N_{33}(f)$
1	0.975	0.975	0.02	0.02	0.78	0.78	0.22	0.22
2	0.91	0.91	0.1	0.1	0.58	0.58	0.42	0.42
3	0.85	0.85	0.19	0.19	0.52	0.52	0.48	0.48

a rotating ground glass diffuser (RGGD) through a translating lens L_2 to generate a spatially incoherent source. The RGGD and SWP are placed at the front and back focal plane of lens L_3, respectively, such that a partially spatially coherent beam falls at the SWP by the consequences of van Cittert–Zernike theorem [45]. The generated partially coherent beam follows the Gaussian statistics, which is following the theoretical assumptions. The correlation width at the SWP can be obtained as $\delta = \frac{3.832\lambda f_3}{2\pi a}$, where f_3 is the focal length of lens L_3 and a is the spot size on RGGD [46]. The correlation between two spatial points at the SWP plane can be manipulated by changing the spot size at RGGD by translating lens L_2. The SWP encodes the requisite polarization on the input beam while maintaining unit DOP across the beam cross section. The generated PC-VVB is focused using lens L_4 at the Stokes camera (SC) plane. The input polarizer (P) is used to change the initial polarization of the beam to obtain different types of PC-VVBs, which are SS degenerate. An additional half-wave plate (HWP) is used to generate a negative topological index PC-VVB [47]. The Stokes parameters ($S_n, n = 0, 1, 2, 3$) of PC-VVBs are recorded simultaneously using SC (SALSA, Bossa Nova Technologies, USA, 1040 × 1040). The PC-VVB of $|\eta| = 1$ and $|\eta| = 2$ are generated using SWPs of $q = 1$ and $q = 2$, respectively (SWP, Thorlabs), while a PC-VVB

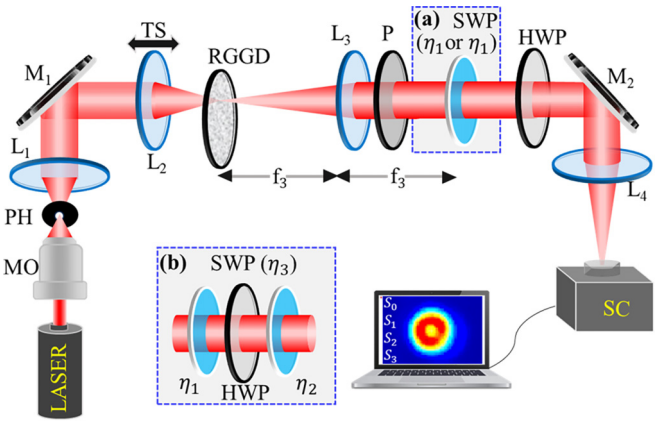

FIG. 3. Schematic of the experimental setup to generate PC-VVBs and investigate the effect of focusing on the Stokes scintillation. MO: microscope objective; PH: pinhole; L_1, L_2, L_3, L_4: lens; M_1, M_2: mirrors; TS: translational stage; RGGD: rotating ground glass diffuser; P: polarizer; HWP: half-wave plate; SWP: spatially varying HWP; SC: Stokes camera. Translating lens L_2 provides a controlled generation of PC-VVBs. The VVB of $|\eta| = 3$ is generated using two SWPs of $|\eta| = 1$ and $|\eta| = 2$ in concatenation with a HWP as shown in the inset (blue-dashed borderline).

of $|\eta| = 3$ was generated using SWPs of $q = 1$ and $q = 2$ in concatenation with HWP [48] (see blue-dashed borderline inset of Fig. 3).

V. RESULTS AND DISCUSSION

Following the Gaussian statistics, the normalized SS parameters are measured at the focal plane (SC plane) using the Stokes parameters as [9]

$$D^N_{00}(\mathbf{r}, f) = \frac{\langle S_0\rangle^2 + \langle S_1\rangle^2 + \langle S_2\rangle^2 + \langle S_3\rangle^2}{2\langle S_0\rangle^2}, \tag{14a}$$

$$D^N_{11}(\mathbf{r}, f) = \frac{\langle S_0\rangle^2 + \langle S_1\rangle^2 - \langle S_2\rangle^2 - \langle S_3\rangle^2}{2\langle S_0\rangle^2}, \tag{14b}$$

$$D^N_{22}(\mathbf{r}, f) = \frac{\langle S_0\rangle^2 - \langle S_1\rangle^2 + \langle S_2\rangle^2 - \langle S_3\rangle^2}{2\langle S_0\rangle^2}, \tag{14c}$$

$$D^N_{33}(\mathbf{r}, f) = \frac{\langle S_0\rangle^2 - \langle S_1\rangle^2 - \langle S_2\rangle^2 + \langle S_3\rangle^2}{2\langle S_0\rangle^2}. \tag{14d}$$

From Eq. (14a), $D^N_{00}(\mathbf{r}, f)$ is directly related to DOP($\mathbf{P}$) of the input beam as in Ref. [49], $D^N_{00}(\mathbf{r}, f) = \frac{1}{2}(1 + \mathbf{P}^2)$, $\mathbf{P} = \frac{\sqrt{\langle S_1\rangle^2+\langle S_2\rangle^2+\langle S_3\rangle^2}}{\langle S_0\rangle}$. Two important bound conditions under Gaussian statistics are [50,51]

$$0.5 \leqslant \mathbf{D}^N_{00}(\mathbf{r}, f) \leqslant 1,$$

$$\sum_{n=0}^{3} D^N_{nn}(\mathbf{r}, f) = 2. \tag{15}$$

The VVBs are inhomogeneously polarized beams, which can be represented on a higher-order Poincaré sphere (HOPS) by a single spatial point, in contrast to the Poincaré sphere, where it is distributed all across the equatorial plane [52]. In Fig. 4, for two correlation widths $\delta_1 = 1.54$ mm and $\delta_2 = 0.85$ mm, we plot theoretically (T) and experimentally (E) obtained SS parameters for PC-VVBs ($|\eta| = 1, 2, 3$) of all four types. The total intensity (S_0), Stokes components distributions ($|S_1|, |S_2|$) are given in the insets for $|\eta| = 1, 2, 3$ with blue, red, and green dotted boxes, respectively. The different inner-spherical shells of HOPS correspond to correlation-induced depolarization effects on various index ($|\eta| = 1, 2, 3$) PC-VVBs. The mentioned DOP values on HOPS directly give the intensity scintillation in the particular PC-VVB. The inner spherical shells shrink more rapidly for higher-index PC-VVBs with reducing δ. This implies that the intensity scintillations can be minimized by reducing δ for higher-order PC-VVBs. From Eqs. (14a)–(14d), it is clear that the azimuthally symmetric and asymmetric distribution of SS parameters is due to the petal-like distribution of Stokes parameters $|S_1|$ and $|S_2|$, since S_3 for PC-VVBs is almost zero. The azimuthal asymmetry of D^N_{11} and D^N_{22} carry information of PHI of the input beam such that (number of petals $K = 4|\eta|$), as discussed in Sec. III. The SS distribution is unchanged on reducing correlation, but their magnitude deteriorates uniformly across the beam cross section. The significant deterioration for higher-index PC-VVBs makes them more robust toward atmospheric turbulent scintillation, which may enhance the information preservation during free space communication [53]. The state of polarization (SOP)

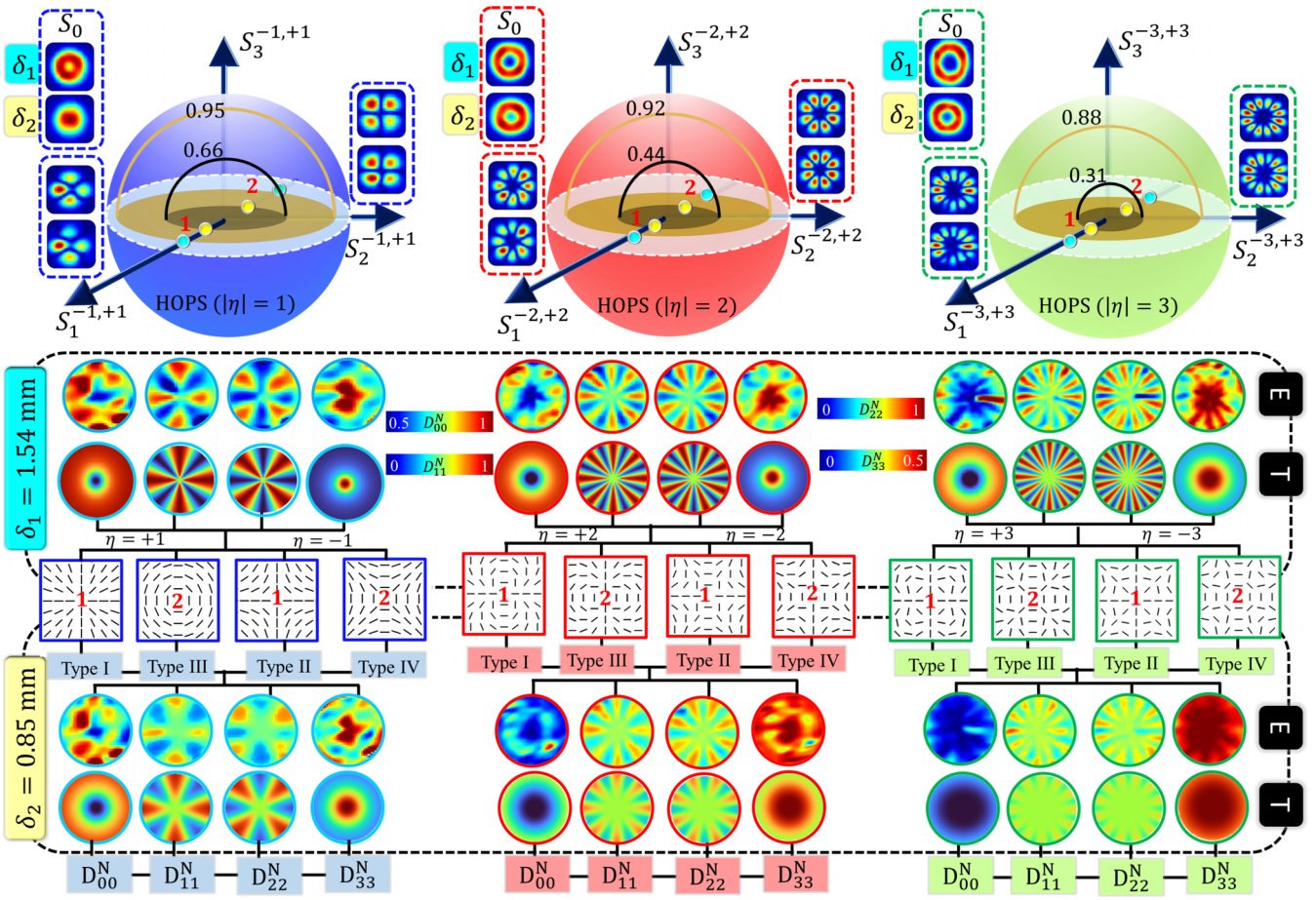

FIG. 4. Higher-order Poincaré sphere representation of focused PC-VVBs $|\eta| = 1$ (blue), $|\eta| = 2$ (red), and $|\eta| = 3$ (green). The experimentally obtained total intensity (S_0), $|S_1|$, and $|S_2|$ for $\delta_1 = 1.54$ mm (cyan), $\delta_2 = 0.85$ mm (yellow) are shown in the blue, red, and green dashed box for $|\eta| = 1, 2, 3$, respectively, in row I. The location of two orthogonal pairs (I, III and II, IV) of PC-VVBs are at diametrically opposite coordinate points of HOPS (points 1 and 2). Inner spherical shells can see the correlation-induced depolarization. The theoretical and experimentally obtained SS parameters at two $\delta's$ are shown in rows II and IV. The SOP distributions for a particular $|\eta|$ in row III show SS degeneracy.

distributions for all four types of PC-VVBs are independent of the correlation-induced depolarization effect. The points 1 and 2 inside the HOPS represent two orthogonal pairs of beams lying at diametrically opposite coordinates. The SS parameters for all four types (for generic PC-VVB: radial, azimuthal, antiradial, and antiazimuthal) of PC-VVBs for particular $|\eta|$ are degenerate (see row IV).

To visualize the variation of SS parameters across the beam cross section, the line profiles are plotted in Fig. 5. It can be seen from the figure that D^N_{00} and D^N_{11} are minimum at the core while increasing toward the edge of the beam. An opposite trend is followed by D^N_{33} and D^N_{22} owing to the complementarity. Thus, the later SS parameters are maximum at the core and decrease toward the edge of the beam. D^N_{00}/D^N_{11} and D^N_{22}/D^N_{33} are minimized for generic PC-VVBs across the beam cross section. However, these parameters can be reduced substantially for higher indices by reducing δ since a reduced two-point correlation is more effective for higher index PC-VVBs, which can be observed by an almost flat green line profile (see Fig. 5 for D^N_{00} and D^N_{11} line profiles). The experimentally obtained maximum values of Stokes scintillations are presented in Table II. It infers that the SS parameters can be optimized using the index and spatial correlation width of the input beam. For instance, D^N_{00} and D^N_{11} are lowered by decreasing spatial correlation and increasing the index at the expense of an increase in D^N_{22} and D^N_{33}. Changing δ and η are two specific ways to squeeze the Stokes scintillations for PC-VVBs. The averaged value of Stokes parameters is obtained by repeating the measurements five times, and the statistical error shown in Fig. 5 is the standard deviation present in the realized data. Along with the bound conditions given in Eq. (15), the spatial correlation, PHI, and the

TABLE II. The experimentally obtained maximum values of SS parameters across the beam cross section for various index PC-VVBs with $|\eta| = 1, 2, 3$ at $\delta_1 = 1.54$ mm and $\delta_2 = 0.85$ mm.

	$\delta_1 = 1.54$ mm				$\delta_2 = 0.85$ mm			
$\lvert\eta\rvert$	$D^N_{00}(f)$	$D^N_{11}(f)$	$D^N_{22}(f)$	$D^N_{33}(f)$	$D^N_{00}(f)$	$D^N_{11}(f)$	$D^N_{22}(f)$	$D^N_{33}(f)$
1	0.96	0.95	0.07	0.08	0.75	0.7	0.3	0.27
2	0.92	0.91	0.08	0.12	0.62	0.6	0.37	0.32
3	0.86	0.88	0.12	0.18	0.55	0.56	0.41	0.45

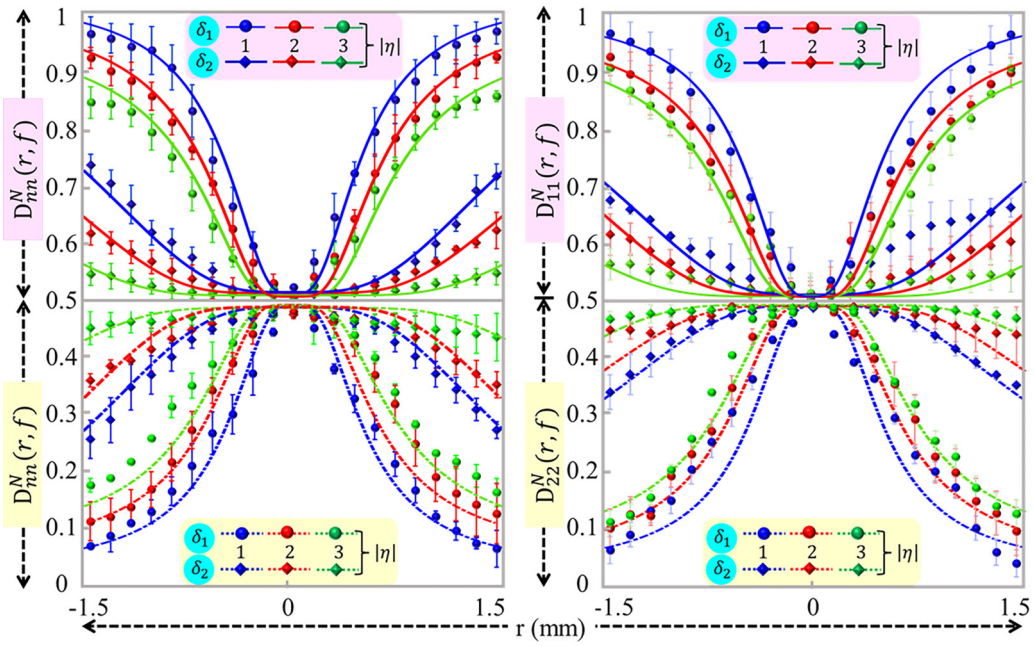

FIG. 5. Variation of SS parameters for PC-VVBs with $|\eta| = 1$ (blue), $|\eta| = 2$ (red), and $|\eta| = 3$ (green) across the beam cross section for different input spatial correlation values ($\delta_1 = 1.54$ mm, $\delta_2 = 0.85$ mm). The solid and dashed lines are theoretical predictions, and various shapes are the experimentally obtained data points.

complementarity of SS parameters may play an essential role in *scintillation squeezing*, the term used as an analogy to the well-known effect of quantum domain [34].

VI. CONCLUSION

In this article, we have studied the Stokes scintillation (SS) parameters for focused vector vortex beams (VVB) of various indices ($|\eta| = 1, 2, 3$) with controlled spatial correlation. The source and observation plane distributions of SS parameters verified their evolution upon focusing. It is found that the SS parameters are modulated by input index, spatial correlation, and focusing of the beam. The distributions of Stokes parameters ($|S_1|$, $|S_2|$) result in both the azimuthal symmetry and asymmetry of SS parameters, which is useful in detection. Owing to the bound conditions of the SS parameter, the change in the input correlation and index give rise to the scintillation squeezing. A uniform deterioration in the Stokes scintillations across the beam cross section is a signature of a deteriorated two-point correlation at the source plane. This research holds particular significance for optical communication systems in both the classical and quantum domains, where intensity and polarization-resolved scintillations play a significant role in signal deterioration.

ACKNOWLEDGMENTS

The research leading to the results presented in this paper has received funding from the Department of Science and Technology, India (DST/ICPS/QUEST/Theme-I/2019). Manisha and H.K.S. acknowledge the financial support of the Senior Research Fellowship (SRF) from the DST, India, and the University Grants Commission (UGC), India, respectively.

APPENDIX: THE CSD ELEMENTS USING EQ. (13)

$$W_{xx}(\mathbf{r}_1,\mathbf{r}_2,f) = -\Pi(r_1,r_2)\sum_{l=-\infty}^{\infty}\sum_{j=0}^{\infty}\left[\frac{P_1(p_1,l)P_2(p_1,l)}{j!\Gamma(a_1)(2\delta^2)^{2j+|l-q|}} + \frac{P_1(p_2,l)P_2(p_2,l)}{j!\Gamma(a_2)(2\delta^2)^{2j+|l+q|}} + \frac{i^{2q}e^{i2q\theta_2}P_1(p_1,l)P_2(p_1,l-2q)}{j!\Gamma(a_1)(2\delta^2)^{2j+|l-q|}} + \frac{i^{-2q}e^{-i2q\theta_2}P_1(p_2,l)P_2(p_2,l+2q)}{j!\Gamma(a_2)(2\delta^2)^{2j+|l+q|}}\right]e^{il(\theta_1-\theta_2)}, \tag{A1}$$

$$W_{yy}(\mathbf{r}_1,\mathbf{r}_2,f) = \Pi(r_1,r_2)\sum_{l=-\infty}^{\infty}\sum_{j=0}^{\infty}\left[-\frac{P_1(p_1,l)P_2(p_1,l)}{j!\Gamma(a_1)(2\delta^2)^{2j+|l-q|}} - \frac{P_1(p_2,l)P_2(p_2,l)}{j!\Gamma(a_2)(2\delta^2)^{2j+|l+q|}} + \frac{i^{2q}e^{i2q\theta_2}P_1(p_1,l)P_2(p_1,l-2q)}{j!\Gamma(a_1)(2\delta^2)^{2j+|l-q|}} + \frac{i^{-2q}e^{-i2q\theta_2}P_1(p_2,l)P_2(p_2,l+2q)}{j!\Gamma(a_2)(2\delta^2)^{2j+|l+q|}}\right]e^{il(\theta_1-\theta_2)}, \tag{A2}$$

$$W_{xy}(\mathbf{r}_1,\mathbf{r}_2,f)=i\Pi(r_1,r_2)\sum_{l=-\infty}^{\infty}\sum_{j=0}^{\infty}\left[\frac{P_1(p_1,l)P_2(p_1,l)}{j!\Gamma(a_1)(2\delta^2)^{2j+|l-q|}}-\frac{P_1(p_2,l)P_2(p_2,l)}{j!\Gamma(a_2)(2\delta^2)^{2j+|l+q|}}+\frac{i^{2q}e^{i2q\theta_2}P_1(p_1,l)P_2(p_1,l-2q)}{j!\Gamma(a_1)(2\delta^2)^{2j+|l-q|}}\right.$$
$$\left.-\frac{i^{-2q}e^{-i2q\theta_2}P_1(p_2,l)P_2(p_2,l+2q)}{j!\Gamma(a_2)(2\delta^2)^{2j+|l+q|}}\right]e^{il(\theta_1-\theta_2)}, \tag{A3}$$

$$W_{yx}(\mathbf{r}_1,\mathbf{r}_2,f)=W_{xy}^{*}(\mathbf{r}_1,\mathbf{r}_2,f). \tag{A4}$$

The functions used in Eqs. (A1)–(A4) are

$$M=\frac{1}{4w^2}+\frac{1}{2\delta^2},$$
$$p_{1/2}=2j+|l\mp q|+q+2,$$
$$a_{1/2}=j+|l\mp q|+1, \tag{A5}$$

$$\Pi(\mathbf{r}_1,\mathbf{r}_2)=\frac{k^2}{8\pi f^2(2w)^{2|q|}}\exp\left[-\frac{k^2r_1^2}{4Mf^2}-\frac{k^2r_2^2}{4Mf^2}\right], \tag{A6}$$

$$P_1(s,t)=\frac{M^{-s/2}}{2t!}\Gamma\left(\frac{s+t}{2}\right)\left(\frac{k^2r_1^2}{4Mf^2}\right)^2\times{}_1F_1\left(\frac{t-s}{2};t+1;\frac{k^2r_1^2}{4Mf^2}\right), \tag{A7}$$

$$P_2(s,t)=\frac{M^{-s/2}}{2t!}\Gamma\left(\frac{s+t}{2}\right)\left(\frac{k^2r_2^2}{4Mf^2}\right)^2\times{}_1F_1\left(\frac{t-s}{2};t+1;\frac{k^2r_2^2}{4Mf^2}\right). \tag{A8}$$

The special notations $\Gamma(\cdot)$ and ${}_1F_1(.;.;.)$ are Gamma function and Kummer functions, respectively. In solving the above expressions, we have used the following expansions and integrals [54,55]:

$$\exp\left[\frac{ik\rho_1r_1}{f}\cos(\theta_1-\phi_1)\right]=\sum_{l=-\infty}^{\infty}i^lJ_l\left(\frac{k\rho_1r_1}{f}\right)e^{il(\theta_1-\phi_1)}, \tag{A9}$$

$$\int_0^{2\pi}\exp[-in\phi_1+N\rho_1\rho_2\cos(\phi_1-\phi_2)]=2\pi\quad\exp(-in\phi_2)I_n(N\rho_1\rho_2), \tag{A10}$$

$$I_n(N\rho_1\rho_2)=\sum_{j=0}^{\infty}\frac{1}{j!\Gamma(j+|n|+1)}\left(\frac{N\rho_1\rho_2}{2}\right)^{2j+|n|}, \tag{A11}$$

$$\int_0^{\infty}r^n\exp(-Sr^2)J_l(\mu r)dr=\frac{\mu^l\Gamma[l+n+1)/2]}{2^{l+1}S^{(l+n+1)/2}\Gamma(l+1)}\,{}_1F_1\left(\frac{l+n+1}{2}:l+1;\frac{-\mu^2}{4S}\right), \tag{A12}$$

$${}_1F_1(x:y;z)=e^z\,{}_1F_1(y-x:y;-z). \tag{A13}$$

Here, $J_l(\cdot)$ is the lth-order Bessel function of the first kind, and $I_n(\cdot)$ is the nth-order modified Bessels function of the first kind.

[1] E. Wolf, *Introduction to the Theory of Coherence and Polarization of Light* (Cambridge University, Cambridge, 2007).
[2] R. H. Brown and R. Q. Twiss, Nature (London) **177**, 27 (1956).
[3] R. Hanbury Brown, *The Intensity Interferometer. Its Applications to Astronomy* (Taylor & Francis, London, 1974).
[4] R. H. Brown and R. Q. Twiss, London, Edinburgh Dublin Philos. Mag. J. Sci. **45**, 663 (1954).
[5] G. Baym, preprint arXiv:nucl-th/9804026 (1998).
[6] T. Shirai and E. Wolf, Opt. Commun. **272**, 289 (2007).
[7] T. Hassinen, J. Tervo, T. Setälä, and A. T. Friberg, Opt. Express **19**, 15188 (2011).
[8] A. Öttl, S. Ritter, M. Köhl, and T. Esslinger, Phys. Rev. Lett. **95**, 090404 (2005).
[9] D. Kuebel and T. D. Visser, J. Opt. Soc. Am. A **36**, 362 (2019).
[10] I. Hajnsek, E. Pottier, and S. R. Cloude, IEEE Trans. Geosci. Remote Sens. **41**, 727 (2003).
[11] R. Hendriks, M. Van Exter, J. Woerdman, L. Weegels, and A. Van Geelen, J. Opt. Soc. Am. B **16**, 832 (1999).
[12] D. F. James, J. Opt. Soc. Am. A **11**, 1641 (1994).
[13] O. Korotkova, Opt. Commun. **281**, 2342 (2008).
[14] J. Wu and L. Song, *2016 8th International Conference on Computational Intelligence and Communication Networks (CICN)* (IEEE, New York, 2016), pp. 129–133.
[15] O. Korotkova and E. Wolf, Opt. Commun. **246**, 35 (2005).
[16] X. Zhao, T. D. Visser, and G. P. Agrawal, Opt. Lett. **43**, 2344 (2018).
[17] B. Kanseri, *Optical Coherence and Polarization: An Experimental Outlook: Experimental Study of Coherence and Polarization Properties of Optical Fields* (LAP Lambert Academic Publishing, London, 2013).
[18] X. Liu, J. Zeng, and Y. Cai, Adv. Phys.: X **4**, 1626766 (2019).
[19] Manisha, S. Joshi, S. N. Khan, B. Kanseri, and P. Senthilkumaran, Opt. Express **30**, 32230 (2022).
[20] P. Senthilkumaran, *Singularities in Physics and Engineering* (IOP Publishing, Bristol, 2024).
[21] S. Ngcobo, I. Litvin, L. Burger, and A. Forbes, Nat. Commun. **4**, 2289 (2013).

[22] M. Dong, D. Jiang, N. Luo, and Y. Yang, Appl. Phys. B **125**, 55 (2019).
[23] K. Khare, P. Lochab, and P. Senthilkumaran, *Orbital Angular Momentum States of Light: Propagation Through Atmospheric Turbulence* (IOP Publishing, Bristol, 2020).
[24] W. Cheng, J. W. Haus, and Q. Zhan, Opt. Express **17**, 17829 (2009).
[25] P. Lochab, P. Senthilkumaran, and K. Khare, Phys. Rev. A **98**, 023831 (2018).
[26] D. P. Brown and T. G. Brown, Opt. Express **16**, 20418 (2008).
[27] J. Yu, Y. Huang, F. Wang, X. Liu, G. Gbur, and Y. Cai, Opt. Express **27**, 26676 (2019).
[28] L. Zhao, Y. Xu, and S. Yang, Optik **227**, 166115 (2021).
[29] F. Wang, Y. Cai, Y. Dong, and O. Korotkova, Appl. Phys. Lett. **100**, 051108 (2012).
[30] Y. Cai, Y. Chen, and F. Wang, J. Opt. Soc. Am. A **31**, 2083 (2014).
[31] S. Joshi, S. N. Khan, P. Senthilkumaran, and B. Kanseri, Phys. Rev. A **103**, 053502 (2021).
[32] H. Rubinsztein-Dunlop *et al.*, J. Opt. **19**, 013001 (2017).
[33] Y. Chen, F. Wang, and Y. Cai, Adv. Phys.: X **7**, 2009742 (2022).
[34] Y. Wang, S. Yan, D. Kuebel, and T. D. Visser, Phys. Rev. A **100**, 023821 (2019).
[35] H. K. Singh, G. Arya, and B. Kanseri, J. Opt. **25**, 014001 (2023).
[36] Z. Dong, B. Yuan, Y. Liu, F. Wang, Y. Cai, and Y. Chen, Chin. Opt. Lett. **21**, 100101 (2023).
[37] J. Xu, Y. Gao, Y. Cai, and T. D. Visser, Photonics **10**, 604 (2023).
[38] T. Setälä, J. Tervo, and A. T. Friberg, Opt. Lett. **31**, 2208 (2006).
[39] L. Mandel and E. Wolf, *Optical Coherence and Quantum Optics* (Cambridge University, Cambridge, 1995).
[40] B. B. Ram, A. Sharma, and P. Senthilkumaran, Opt. Lett. **42**, 3570 (2017).
[41] T. D. Visser, G. Gbur, and E. Wolf, Opt. Commun. **213**, 13 (2002).
[42] D. G. Fischer and T. D. Visser, J. Opt. Soc. Am. A **21**, 2097 (2004).
[43] X. Zhao, T. D. Visser, and G. P. Agrawal, J. Opt. Soc. Am. A **35**, 1518 (2018).
[44] J. W. Goodman, *Introduction to Fourier Optics* (Roberts and Company, Doylestown, 2005).
[45] B. Kanseri and H. K. Singh, Optik **206**, 163747 (2020).
[46] J. T. Foley, J. Opt. Soc. Am. A **8**, 1099 (1991).
[47] S. K. Pal, Ruchi, and P. Senthilkumaran, Appl. Opt. **56**, 6181 (2017).
[48] S. Delaney, M. M. Sánchez-López, I. Moreno, and J. A. Davis, Appl. Opt. **56**, 596 (2017).
[49] T. Setälä, K. Lindfors, M. Kaivola, J. Tervo, and A. T. Friberg, Opt. Lett. **29**, 2587 (2004).
[50] X. Liu, G. Wu, X. Pang, D. Kuebel, and T. D. Visser, J. Mod. Opt. **65**, 1437 (2018).
[51] A. T. Friberg and T. D. Visser, Opt. Commun. **335**, 82 (2015).
[52] G. Milione, H. I. Sztul, D. A. Nolan, and R. R. Alfano, Phys. Rev. Lett. **107**, 053601 (2011).
[53] Y. Baykal, Opt. Commun. **386**, 53 (2017).
[54] G. B. Arfken, H. J. Weber, and F. E. Harris, *Mathematical Methods for Physicists: A Comprehensive Guide* (Academic, New York, 2011).
[55] A. Jeffrey and H. H. Dai, *Handbook of Mathematical Formulas and Integrals* (Elsevier, New York, 2008).